Supporting Information

Superhydrophobic wood aerogel for radiative cooling and sound absorption

*A-Jun Chang, [a] Chao-Hua Xue, [*a] Jiao-Jiao Sun, [a] Jun Cheng, [*b] Meng-Chen Huang, [c] Bing-Ying Liu, [a] Hui-Di Wang, [a] Xiao-Jing Guo, [a] Chao-Qun Ma, [a] Li-Wan, [a], Yong-Gang Wu,[a] Yan-Yan Yan [a]*

[a] College of Bioresources Chemical and Materials Engineering, Shaanxi University of Science & Technology, Xi'an 710021, China. E-mail: xuech@.sust.edu.cn

[b] Northwest Institute for Nonferrous Metal Research, Shaanxi Key Laboratory of Biomedical Metal Materials, Xi'an 710016, China. E-mail: chengjun_851118@126.com

[c] School of Manufacture Science and Engineering, Southwest University of Science and Technology, Mianyang 621010, China.

Note S1: Theoretically Calculated Radiative Cooling Power of WA

The net cooling power (P_{net}) is expressed as:

$$P_{net} = P_{rad} - P_{atm} - P_{sun} - P_{cond+conv} \quad (1)$$

where P_{rad} is the radiative power emitted from WA, calculated by:

$$P_{rad} = \int d\Omega \cos\theta \int I_{BB}(T_{rad}, \lambda)\, \varepsilon(\lambda, \theta) d\lambda \quad (2)$$

Where, $\int d\theta = 2\pi \int_0^{\frac{\pi}{2}} \sin\theta d\theta$ is the hemispherical angular integral, $\varepsilon(\lambda, \theta)$ is the emissivity of WA as a function of wavelength (λ) and incident angle (θ), $\int I_{BB}(T_{rad}, \lambda) = \frac{2hc^2}{\lambda^5} \cdot \frac{1}{e^{\frac{hc}{\lambda k_b T_{rad}}} - 1}$ is the spectral irradiance emitted by a blackbody, where T_{rad} is the temperature of radiative coolers, c is the light speed, h is the Plank constant and k_b is the Boltzmann constant. P_{atm} is the absorbed atmospheric radiation, calculated by:

$$P_{atm} = \int d\Omega \cos\theta \int I_{BB}(T_{amb}, \lambda)\, \varepsilon(\lambda, \theta) \varepsilon_{atm}(\lambda, \theta) d\lambda \quad (3)$$

in which, T_{amb} is the temperature of ambient air, $\varepsilon_{atm}(\lambda, \theta) = 1 - [\tau_{atm}(\lambda, \theta)]^{\frac{1}{\cos\theta}}$ is the spectral directional emissivity of the atmosphere, where $\tau_{atm}(\lambda, \theta)$ represents the atmospheric transmissivity in the vertical direction. P_{sun} is the absorbed solar irradiance, calculated by:

$$P_{sun} = \int I_{AM1.5}(\lambda)\, \varepsilon(\lambda, \theta_{sun}) d\lambda \quad (4)$$

in which, θ_{sun} is the incident angle of the sunlight, $I_{AM1.5}$ is the direct normal spectral solar irradiance ASTM G173 under air-mass 1.5. $P_{cond+conv}$ is the non-radiative power losses, calculated by:

$$P_{cond+conv} = q(T_{amb} - T_{rad}) \quad (5)$$

in which, $q = q_{cond} + q_{conv}$ is the non-radiative heat coefficient composed of thermal conduction and convection.

Fig. S1: WA with lightweight feature.

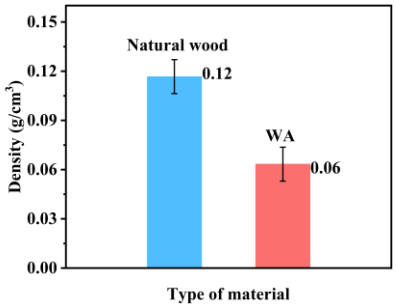

Fig. S2: Compared to natural wood, WA has a density of only 0.06 g/cm^3, which is about half that of natural wood.

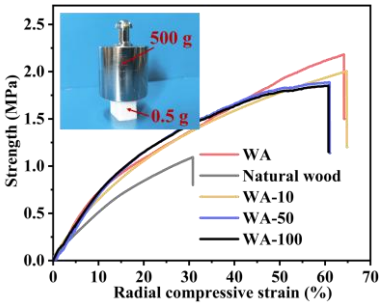

Fig. S3: The radial compressive strength of WA is 2.2 MPa. Even after 100 compression cycles, the strength only drops by 0.25 MPa. The inset shows that a 0.5 g WA can support a 500 g weight.

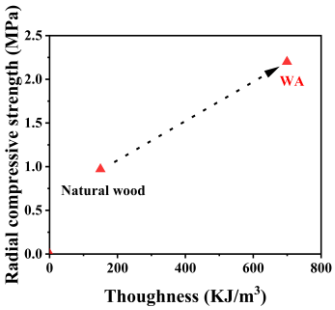

Fig. S4: Measured by the radial compressive strength, WA exhibits higher strength and toughness, increasing from 187 KJ/m^3 in natural wood to 700 KJ/m^3.

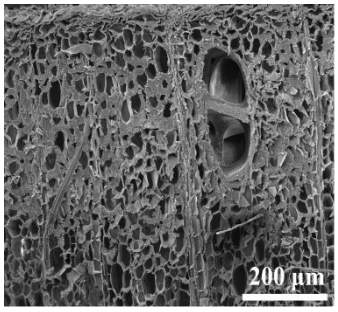

Fig. S5: SEM image of the cross-section of natural wood, revealing a hierarchically porous structure.

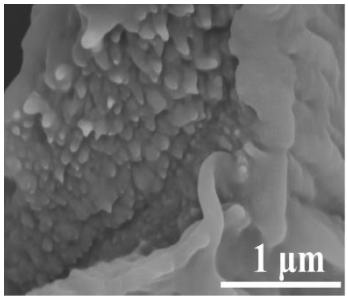

Fig. S6: The composition of the cell wall is mainly composed of cellulose, which mainly improves its mechanical strength and effectively protects the cell from external damage. In addition to cellulose, there is also a part of lignin and hemicellulose in the cell wall, which play a role in connecting other cell walls.

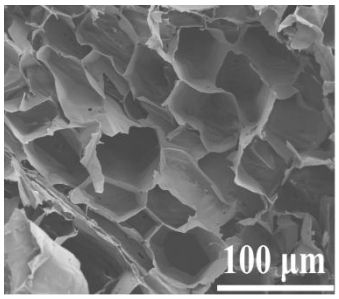

Fig. S7: After delignification and freeze-drying treatment, WA still retains the natural wood vertical directional cylindrical pores. However, unlike natural wood, more cylindrical pores are exposed, and new pores are formed between the cell walls.

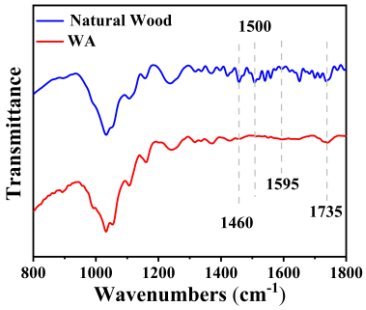

Fig. S8: FTIR spectra of the natural wood and WA.

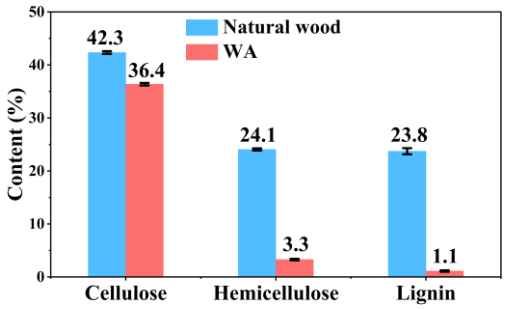

Fig. S9: The relative contents of cellulose, hemicellulose, and lignin in natural wood and WA.

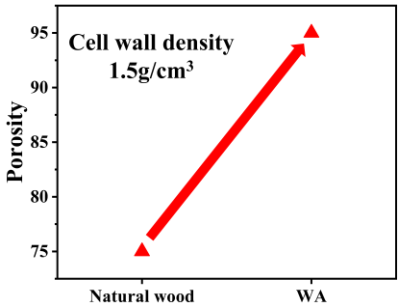

Fig. S10: The porosity of WA and natural wood.

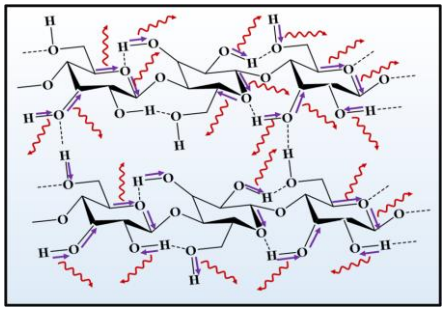

Fig. S11: Schematic diagram of molecular vibration and infrared emission of functional groups in cellulose.

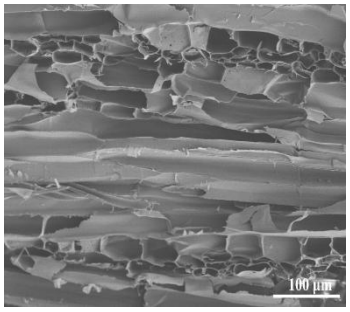

Fig. S12: The cellulose fibers along the growth direction exhibit a multiscale distribution.

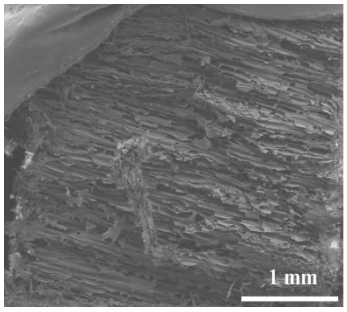

Fig. S13: WA retains the natural conduits of natural wood.

Fig. S14: WA has high reflectance in the visible light range, showing a bright white appearance (right). Natural wood contains lignin, which can absorb visible light, thus showing a yellow appearance (left).

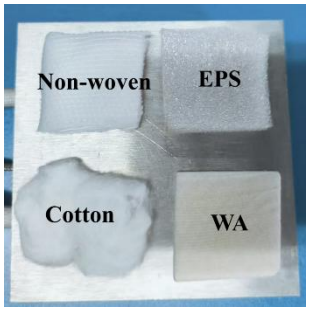

Fig. S15: Digital photograph of various samples heated on a heating stage.

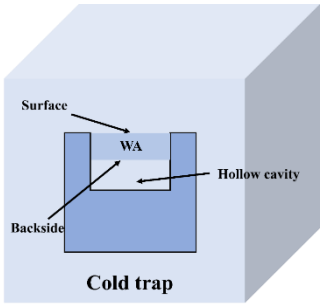

Fig. S16: Schematic diagram of the cold trap test device.

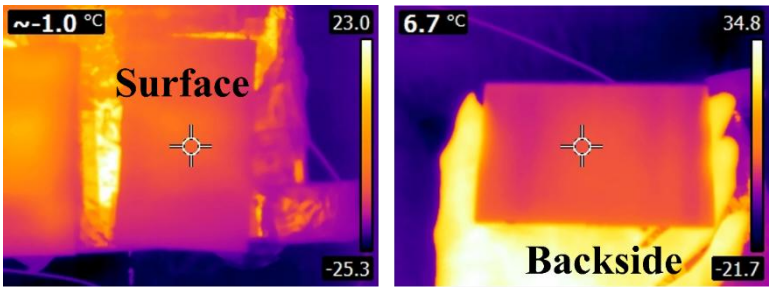

Fig. S17: Infrared photograph of the surface and backside of natural wood.

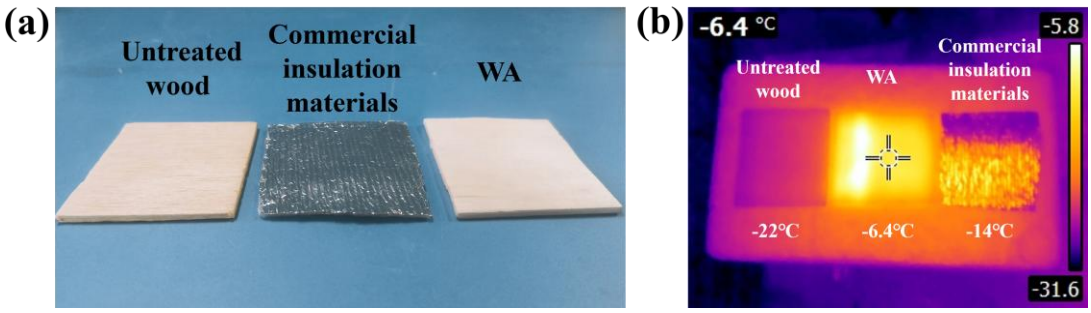

Fig. S18: (a) Digital photos of the samples involved. (b) Infrared photograph captured after being placed in the cold trap for 20 minutes.

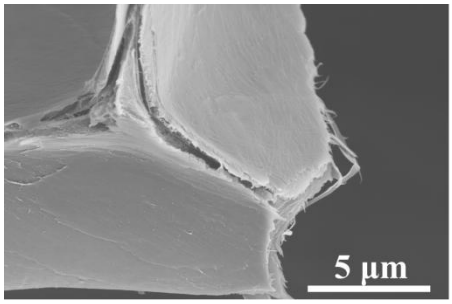

Fig. S19: After delignification treatment, micrometer-scale cracks occur between the fibers.

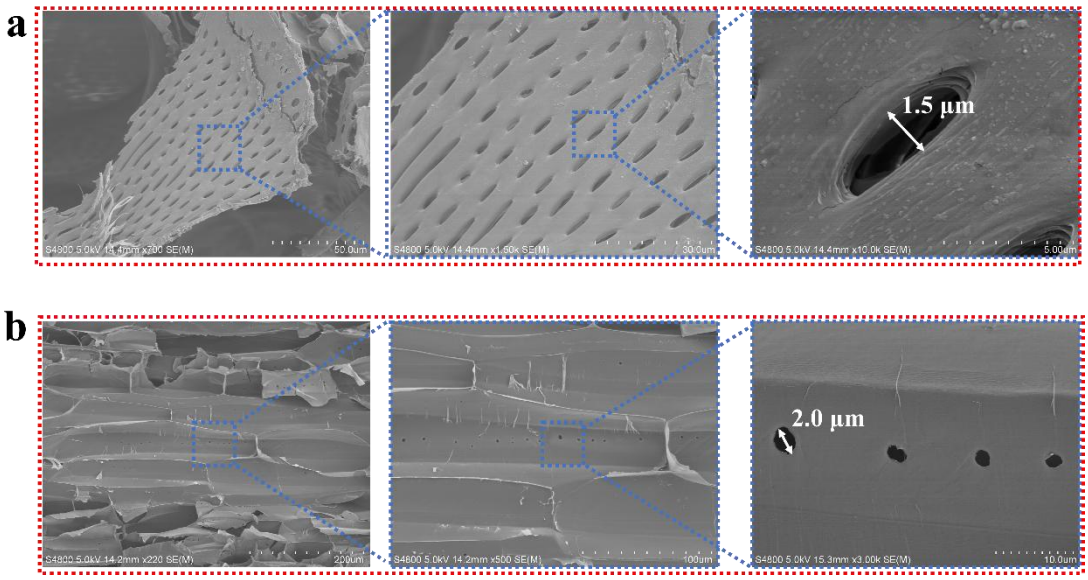

Fig. S20: After delignification treatment, the micro-nano-scale pore and pit structures are exposed.

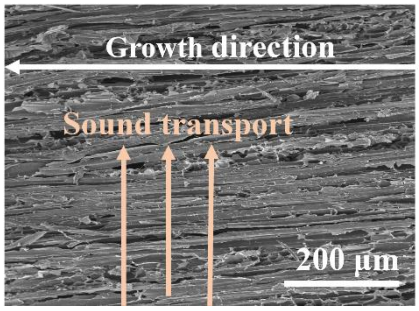

Fig. S21: The direction of sound propagation is perpendicular to the growth direction of the wood.

S22: The average value of environmental noise is 103.1 dB.

Fig. S23: The two houses are constructed with natural wood and WA respectively, and are positioned outdoors where the environmental temperature is 55°C.

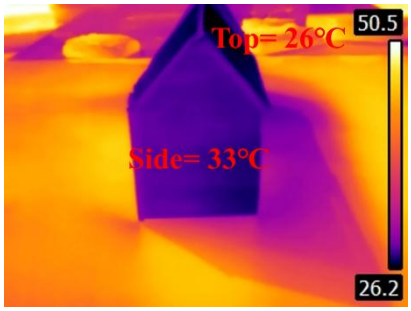

Fig. S24: When the top temperature is 26°C and the side temperature is 33°C. The side temperature is higher than the top temperature, demonstrating a differentiated cooling phenomenon.

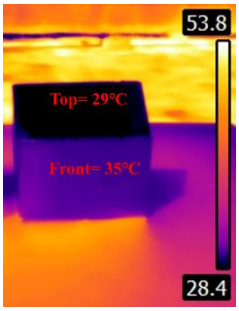

Fig. S25: When the top temperature is 29°C and the frontal temperature is 35°C. The front temperature is higher than the top temperature. It presents a differential cooling effect.

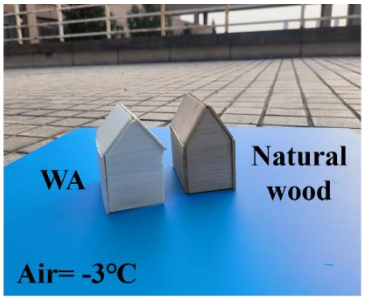

Fig.S26: The two houses are constructed with natural wood and WA respectively, and are positioned outdoors where the environmental temperature is -3°C.

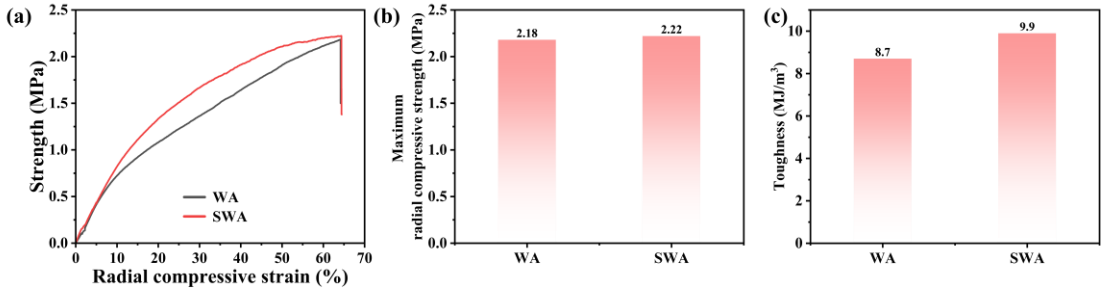

Fig.S27: The stress-strain curves (a), maximum stress (b), and toughness (c) comparisons of WA and SWA.

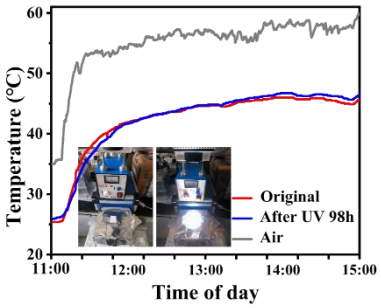

Fig. S28: After 98 hours of ultraviolet aging, the outdoor test presented the cooling curve. Among them, after the aging test, the cooling effect was nearly indistinguishable from that of the original WA (June 13th, 2024).

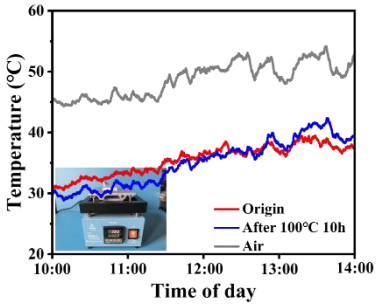

Fig. S29: The SWA outdoor cooling curve after being treated at 100°C for 10 hours was investigated. It was found that the cooling effect was similar to the original WA, suggesting that WA possesses the property of high-temperature resistance (July 21st, 2024).

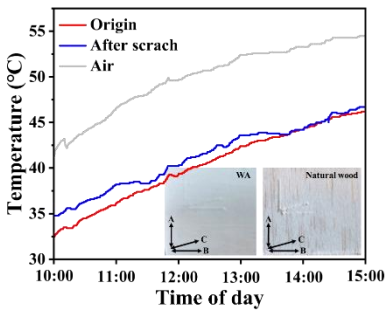

Fig. S30: The outdoor cooling curve of WA after scratch processing was observed. It was discovered that the cooling effect was close to that of the original WA, suggesting that WA has mechanical stability. Among them, A, B, and C respectively represent the directions parallel, perpendicular, and at a 60° angle to the tree growth direction (July 31st, 2024).

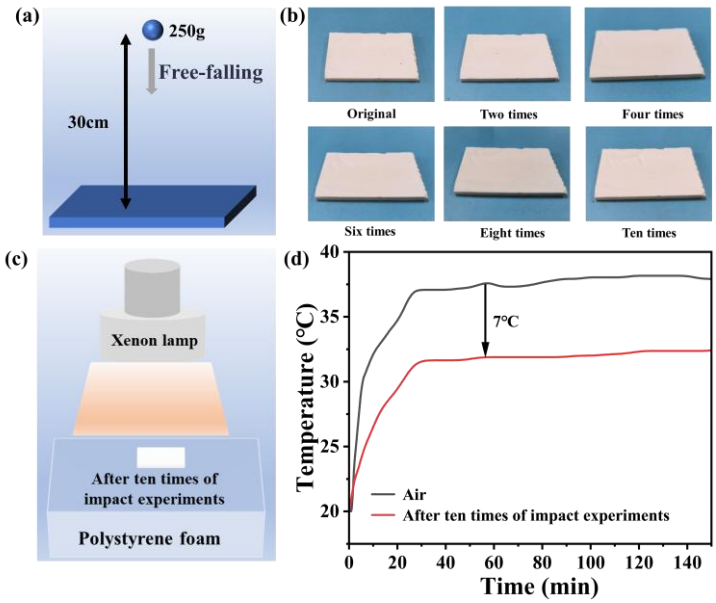

Fig. S31: (a) Schematic diagram of anti-impact experiment. (b) Digital photographs of the sample after undergoing 10 impact experiments. (c) Schematic diagram of indoor xenon lamp simulation. (d) The temperature curve for a continuous 150 minutes.

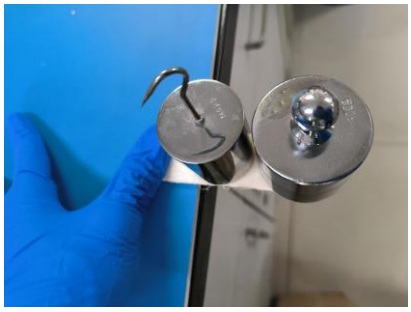

Fig. S32: The bending resistance experiment. One end of WA is fixed, and subsequently pressure is exerted on the other end for 5 minutes. The applied weight is 750g, and the sample size is 7.5cm × 2.5cm × 0.5cm (length × width × thickness).

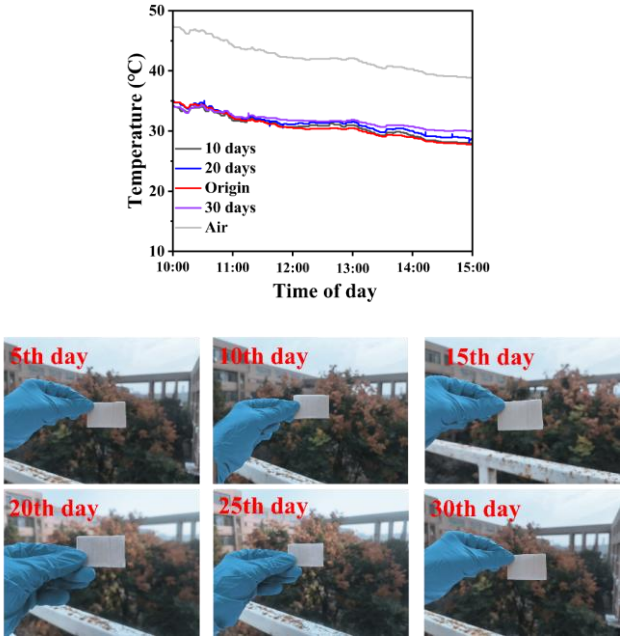

Fig. S33: The cooling curves of SWA after undergoing outdoor exposure for 10 days, 20 days, and 30 days (August 2nd, 2024).

Table S1 Comparison of properties of different materials.

	Density (g/cm^3)	Thermal conductivity (W/m·K)	Reflectivity (%)	Sound absorption coefficient	Strength (Mpa)
WA	0.06	0.043	92	0.40	2.18
SWA	0.07	0.046	93	0.42	2.22
Synthetic fiber	0.98	0.120	30	0.31	0.86
Foam	0.07	0.061	35	0.33	0.66
Glass	2.5	1.100	20	0.08	1.82
Hollow brick	1.0	0.60	23	0.33	2.03

Table S2 Propety changes of WA and SWA after 30 days of outdoor exposure.

	Density (g/cm^3)	Thermal conductivity (W/m·K)	Reflectivity (%)	Sound absorption coefficient	Strength (Mpa)
WA (Before)	0.06	0.043	92	0.40	2.18
SWA(Before)	0.07	0.046	93	0.42	2.22
WA (After)	0.10	0.095	81	0.21	1.53
SWA (After)	0.08	0.047	92	0.41	2.20